Stem Cell Reports
Article

OPEN ACCESS

Characterization of Human Induced Pluripotent Stem Cell-Derived Retinal Pigment Epithelium Cell Sheets Aiming for Clinical Application

Hiroyuki Kamao,[1,2] Michiko Mandai,[1] Satoshi Okamoto,[1] Noriko Sakai,[1] Akiko Suga,[1] Sunao Sugita,[1] Junichi Kiryu,[2] and Masayo Takahashi[1,*]

[1]Laboratory for Retinal Regeneration, RIKEN Center for Developmental Biology, Kobe, Hyogo 650-0047, Japan
[2]Department of Ophthalmology, Kawasaki Medical School, Kurashiki, Okayama 701-0114, Japan
*Correspondence: mretina@cdb.riken.jp
http://dx.doi.org/10.1016/j.stemcr.2013.12.007

SUMMARY

Age-related macular degeneration (AMD) causes severe visual impairment due in part to age-dependent impairment of retinal pigment epithelium (RPE). It has been suggested that autologous human induced pluripotent stem cells (hiPSCs) may represent a useful cell source for the generation of graft RPE. We generated hiPSC-derived RPE (hiPSC-RPE) cell sheets optimized to meet clinical use requirements, including quality, quantity, consistency, and safety. These cell sheets are generated as a monolayer of cells without any artificial scaffolds, express typical RPE markers, form tight junctions that exhibit polarized secretion of growth factors, and show phagocytotic ability and gene-expression patterns similar to those of native RPE. Additionally, upon transplantation, autologous nonhuman primate iPSC-RPE cell sheets showed no immune rejection or tumor formation. These results suggest that autologous hiPSC-RPE cell sheets may serve as a useful form of graft for use in tissue replacement therapy for AMD.

INTRODUCTION

Age-related macular degeneration (AMD) (Bressler et al., 1988) is a leading cause of severe visual impairment in elderly persons in developed countries and is characterized by progressive degeneration of the retinal pigment epithelium (RPE). RPE consists of a monolayer of cells situated between the photoreceptors and the choroid, and plays essential roles in photoreceptor maintenance, such as supplying nutrition, formation of the blood-retinal barrier, and phagocytosis of mature outer rod segments shed by photoreceptors (Young and Bok, 1969), as well as in the maintenance of choroidal circulation by the secretion vascular endothelial growth factor (VEGF) from its basal aspect. Current therapies for AMD show only limited efficacy, and in recent years increasing attention has been given to the replacement of pathological RPE with healthy tissue. To date, transplantation of allogeneic fetal RPE (Algvere et al., 1994) or autologous peripheral RPE (Binder et al., 2002; van Meurs and Van Den Biesen, 2003) has been reported in AMD patients, although neither represents an ideal tissue source; fetal tissue is immunogenic, while the latter requires RPE to be harvested by an invasive procedure. Human induced pluripotent stem cells (hiPSCs) (Takahashi et al., 2007) exhibit a number of clinically attractive features, including the potential to serve as an autologous cell source through reprogramming of a patient's own somatic cells, and the ability to self-renew and expand in culture, and to differentiate into RPE.

In RPE transplantation, it is widely accepted that grafted cells perform better in terms of their morphology, physiology, and survival when transplanted as sheets rather than in suspension. It appears that environmental factors provided by cell sheets, such as extracellular matrix and adhesion molecules, help to prevent apoptosis (Tezel and Del Priore, 1997). Previous studies generated RPE cell sheets using various artificial scaffolds (Bhatt et al., 1994; Lee et al., 2002); however, biodegradable materials may cause inflammation, and nondegradable membranes may separate the RPE from the underlying choroid that nourishes the RPE and photoreceptors. To date, there have been no published reports of RPE cell sheets generated without any artificial scaffold, although cell sheets that do not use an artificial scaffold have been generated from various other cell types, such as cornea (Nishida et al., 2004), cardiac myoblast (Shimizu et al., 2001), and hepatocyte (Harimoto et al., 2002), for use in clinical studies.

We previously reported the induction of RPE from both embryonic stem cells (ESCs) (Haruta et al., 2004; Kawasaki et al., 2002; Osakada et al., 2008; Thomson et al., 1998) and iPSCs (Jin et al., 2012; Hirami et al., 2009). In the present study, we assessed the quality, quantity, consistency, and safety of clinical-grade hiPSC-RPE cell sheets eliminating the need for artificial scaffolds by examining their morphology, function in vitro and in vivo, and gene expression. We additionally compared the immunogenicity of autologous and allogeneic iPSC-RPE grafts in a nonhuman primate.

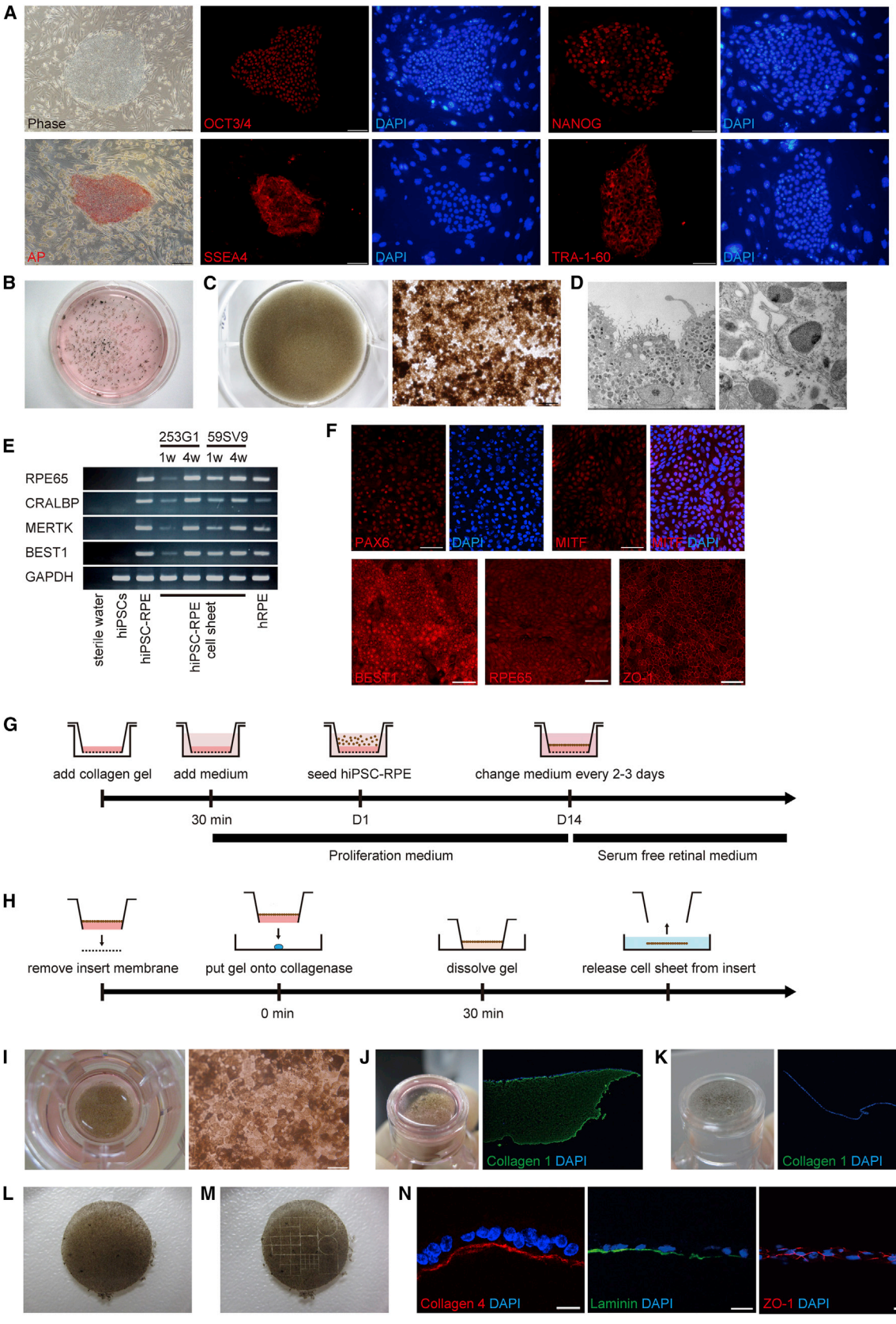

(legend on next page)

RESULTS

Differentiation of hiPSCs into RPE

Using a modified protocol, we induced hiPSC-RPE from hiPSCs (253G1; Nakagawa et al., 2008) that expressed the pluripotency markers OCT3/4, NANOG, SSEA4, TRA-1-60, and alkaline phosphatase (Figure 1A). Three weeks after differentiation was initiated, pigmented colonies with a typical RPE cobblestone appearance formed (Figure 1B). To obtain pure populations of these cells, we manually transferred the pigmented colonies and cultured them until they became confluent (Figure 1C). The pigmented cells had the structural characteristics of RPE including abundant apical microvilli, adherens junctions, and tight junctions under transmission electron microscopy (Figure 1D). Additionally, the pigmented cells expressed typical RPE markers associated with the retinoid cycle (RPE65 [Gu et al., 1997; Marlhens et al., 1997] and CRALBP [Maw et al., 1997]), phagocytosis (MERTK [Gal et al., 2000]), and chloride channels (BEST1 [Stone et al., 1992]) as detected by RT-PCR (Figure 1E), and eye field specification markers (PAX6 and MITF), BEST1, RPE65, and a tight junction marker (ZO-1) on immunocytochemistry (Figure 1F).

Production of hiPSC-RPE Cell Sheets with No Artificial Scaffold

To produce hiPSC-RPE cell sheets without any artificial scaffold, we seeded hiPSC-RPE onto type I collagen gel on a Transwell insert. Typically, hiPSC-RPE became confluent on the collagen gel within 2 weeks after seeding, and confluent hiPSC-RPE formed a pigmented monolayer sheet with a characteristic RPE cobblestone appearance (Figure 1I). One and 4 weeks after reaching confluence, the hiPSC-RPE cell sheets expressed typical RPE markers (RPE65, CRALBP, MERTK, and BEST1) on RT-PCR (Figure 1E).

After the sheets reached confluence, we removed an insert membrane and applied a collagenase from the bottom to dissolve the collagen gel (Figures 1J and 1K), and then cut the margin of the hiPSC-RPE to release it as cell sheet from the insert (Figure 1L). The hiPSC-RPE cell sheets were approximately 1 cm in diameter, which is large enough to cover AMD lesions in the macula about 3 mm in diameter, and retained their sheet structure (Movie S1 available online). The collagen gel initially used as a temporary scaffold was substantively removed by collagenase treatment, as shown by immunohistochemistry (Figures 1J and 1K). The procedure is summarized in Figures 1G and 1H. We prepared grafts by cutting cell sheets into the desired size and shape using a laser microdissection (LMD) system (Figure 1M; Movie S2). These grafts expressed an extracellular matrix of basement membrane (laminin and type IV collagen) and ZO-1 on immunohistochemistry (Figure 1N), and remained intact when subjected to manipulations required for the transplantation procedure (Movie S3).

Figure 1. Generation of hiPSC-RPE and hiPSC-RPE Cell Sheets from hiPSCs

(A) Phase-contrast image and immunostaining for the pluripotency markers OCT3/4, NANOG, SSEA4, TRA-1-60, and alkaline phosphatase of hiPSCs. Scale bar, 200 μm.

(B) Low-power images of a 6 cm dish containing hiPSCs 3 weeks after initiation of differentiation.

(C) Low-power (left panel) and phase-contrast (right panel) images of a 12-well dish containing third-passage hiPSC-RPE 4 weeks after seeding. Scale bar, 200 μm.

(D) Transmission electron microscopy image of abundant apical microvilli (left panel) and adherens and tight junctions (right panel) in the pigmented cells.

(E) RT-PCR analysis of typical RPE markers in iPSCs (253G1), iPSC-RPE (253G1), iPSC-RPE cell sheets (253G1 and 59SV9), and hRPE. hiPSC-RPE cell sheets (253G1 and 59SV9) expressed typical RPE markers 1 week (1w) and 4 weeks (4w) after they reached confluence on collagen gel.

(F) Immunostaining for typical RPE markers (PAX6, MITF, BEST1, RPE65, and ZO-1) in the pigmented cells. Scale bars, 50 μm.

(G) Schematic image showing the procedure for culture of iPSC-RPE on the collagen gel.

(H) Schematic image showing the procedure for iPSC-RPE cell sheets.

(I) Low-power (left panel) and phase-contrast (right panel) images of the Transwell insert containing hiPSC-RPE cell sheets that became confluent on the collagen gel. Scale bars, 50 μm.

(J) Low-power image of the Transwell insert after the insert membrane was removed (left panel). Immunostaining for type I collagen (green) of hiPSC-RPE on the collagen gel before collagenase treatment (right panel). The collagen gel is positive for collagen I (green).

(K) Low-power image of the Transwell insert after collagenase treatment (left panel). Immunostaining for type I collagen (green) of hiPSC-RPE on the collagen gel after collagenase treatment (right panel). The collagen gel is completely eliminated using collagenase I (green) in immunohistochemistry.

(L) Low-power image of a released hiPSC-RPE cell sheet.

(M) Low-power image of grafts made by cutting the cell sheet using the LMD system.

(N) Immunostaining for basement membrane (laminin and type IV collagen) and tight junction (ZO-1) marker in the grafts. Scale bar, 20 μm.

See also Movies S1, S2, and S3.

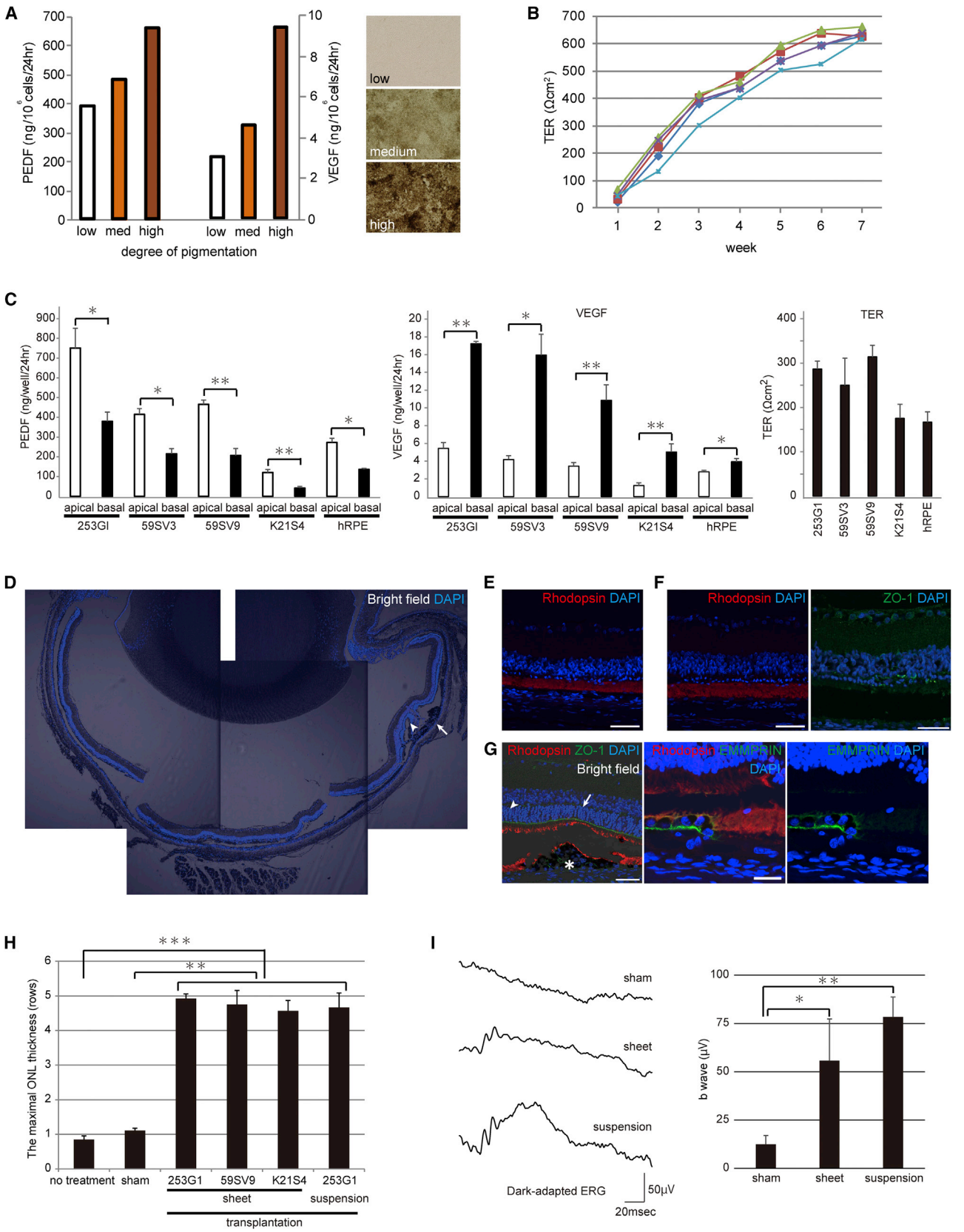

(legend on next page)

Functional Assessment of hiPSC-RPE Cell Sheets In Vitro and In Vivo

We investigated whether the hiPSC-RPE exhibited functions typically observed in native RPE. RPE is known to secrete a range of growth factors, including pigment epithelium-derived factor (PEDF; Steele et al., 1993) and VEGF (Adamis et al., 1993), and to contribute to blood-retinal barrier function. Using ELISA, we measured concentrations of PEDF and VEGF in conditioned hiPSC-RPE medium exhibiting different grades of pigmentation (low, medium, and high). We evaluated barrier function by measuring the transepithelial electrical resistance (TER; Stevenson et al., 1986), which provides a simple and sensitive method for the detection of functional tight junctions. On the dish, hiPSC-RPE secreted PEDF and VEGF, increasing as the intensity of the pigmentation increased (Figure 2A), and hiPSC-RPE on the Transwell insert showed a high TER in a time-dependent manner (Figure 2B). We next measured the TER and concentration of PEDF and VEGF in apical and basal media of hiPSC-RPE grown on the collagen gel in the inserts 4 weeks after they became confluent. The mean TER was approximately 290 Ωcm^2 and the concentration of PEDF was higher in the apical than in the basal medium, whereas that of VEGF was higher in the basal than in the apical medium (Figure 2C). Furthermore, we obtained consistent results with regard to expression of typical RPE markers, polarized secretion of PEDF and VEGF, and high TER with three different hiPSC-RPE lines (59SV3, 59SV9, and K21S4) generated from fibroblasts harvested from a patient with retinitis pigmentosa (RP), as well as from commercially available human fetal RPE (hRPE) used as a control (Figures 1E and 2C).

To assess the function of hiPSC-RPE cell sheets (253G1, 59SV9, and K21) in vivo, we transplanted fragments of sheets into the subretinal space of pink-eyed Royal College of Surgeons (RCS) dystrophic rats, an animal model of inherited retinal degeneration (Mullen and LaVail, 1976). RCS rats carry a mutation in the *Mertk* gene that results in defective phagocytosis of photoreceptor outer segments by RPE, and lose their photoreceptor cells by approximately 3 months after birth (Dowling and Sidman, 1962). It has been reported that transplantation of normal RPE into the subretinal space of RCS rats at an early age preserves photoreceptor cells around the grafted cells (Li and Turner, 1988). We transplanted 1 × 1 mm hiPSC-RPE cell sheets, including 1.42×10^4 cells (live cells: 1.32×10^4

Figure 2. Functional Assessment of hiPSC-RPE Cell Sheets In Vitro and In Vivo

(A) ELISA of PEDF and VEGF secretion by hiPSC-RPE (253G1) on the dish (PEDF: low 386.2, medium 478.5, high 658.1 ng/10^6 cells/24 hr; VEGF: low 3.07, medium 4.6, high 9.38 ng/10^6 cells/24 hr). Right panels show phase-contrast images of hiPSC-RPE exhibiting different grades of pigmentation (upper panel is low pigmentation, middle panel is medium pigmentation, and lower panel is high pigmentation).

(B) TER of five hiPSC-RPE cell sheets (253G1) on Transwell inserts at 7 weeks after seeding.

(C) TER and concentration of PEDF and VEGF in apical and basal media of hiPSC-RPE (253G1, 59SV3, 59SV9, and K21S4) and hRPE on the collagen gel in the Transwell insert. hiPSC-RPE (253G1; n = 3), PEDF: apical 751.0 ± 100.0, basal 379.7 ± 46.4 ng/well/24 hr, VEGF: apical 5.44 ± 0.65, basal 17.22 ± 0.27 ng/well/24 hr, TER: 287 ± 18 Ωcm^2. hiPSC-RPE (59SV3; n = 3), PEDF: apical 415.0 ± 29.7, basal 215.0 ± 25.6 ng/well/24 hr, VEGF: apical 4.18 ± 0.44, basal 15.95 ± 2.33 ng/well/24 hr, TER: 250 ± 61 Ωcm^2. hiPSC-RPE (59SV9; n = 5), PEDF: apical 465.8 ± 21.2, basal 206.8 ± 35.0 ng/well/24 hr, VEGF: apical 3.44 ± 0.39, basal 10.84 ± 1.75 ng/well/24 hr, TER: 314 ± 26 Ωcm^2. hiPSC-RPE (K21S4; n = 9), PEDF: apical 120.0 ± 15.7, basal 40.6 ± 9.2 ng/well/24 hr, VEGF: apical 1.23 ± 0.31, basal 5.03 ± 0.92 ng/well/24 hr, TER: 176 ± 32 Ωcm^2. hRPE (n = 3), PEDF: apical 272.8 ± 20.8, basal 135.8 ± 5.6 ng/well/24 hr, VEGF: apical 2.80 ± 0.16, basal 3.93 ± 0.37 ng/well/24 hr, TER: 167 ± 23 Ωcm^2.

(D) DAPI-stained sections. Images of hiPSC-RPE cell sheet transplantation in a 12-week-old RCS rat, showing preservation of the ONL (arrowhead) around the graft (arrow).

(E–G) Confocal images of RCS rat eyes. Scale bar, 50 μm.

(E) Immunostaining for rhodopsin (red) in nontransplanted eye section.

(F) Immunostaining for rhodopsin (red, left panel) and ZO-1 (green, right panel) in sham-surgery eye section.

(G) Immunostaining for rhodopsin (red) and ZO-1 (green) in transplanted eye section (left panel). The ONL (arrow) situated above the graft (asterisk) was preserved for a thickness of five cell rows, and the ONL (arrowhead) with the debris zone was preserved beyond the border of the graft. Scale bar, 50 μm. Immunostaining for rhodopsin (red) and EMMPRIN (green) in transplanted eye section (center and right panel). The transplanted cell fragment is positive for anti-human EMMPRIN. Scale bar, 20 μm.

(H) Immunohistochemical analyses of 12-week-old RCS rats. The ONL thickness of the hiPSC-RPE cell sheet (253G1; n = 27; 59SV9; n = 12; K21S4; n = 7) and cell suspension (n = 6) in the transplanted eyes was significantly greater than in either the sham (n = 27) or non-transplanted (n = 13) eyes. The ONL situated above transplanted cells was five cell rows. In contrast, the ONL in the eyes without transplantation was almost completely lost.

(I) Left panel: average scotopic responses to single flashes were recorded in 9-week-old RCS rats after sham injection (13 ± 5 μV; n = 7 eyes) and transplantation of hiPSC-RPE cell sheet (56 ± 22 μV; n = 3 eyes) and cell suspension (78 ± 10 μV; n = 4 eyes). Both transplanted eyes have reduced a- and b-waves, and sham eyes have only a negative component. Right panel: b-wave amplitude of each RCS rat, showing the preventive effect of transplantation.

All pooled data are represented as mean ± SEM; asterisks (*) indicate statistical significance (*$p < 0.05$, **$p < 0.01$, ***$p < 0.001$).

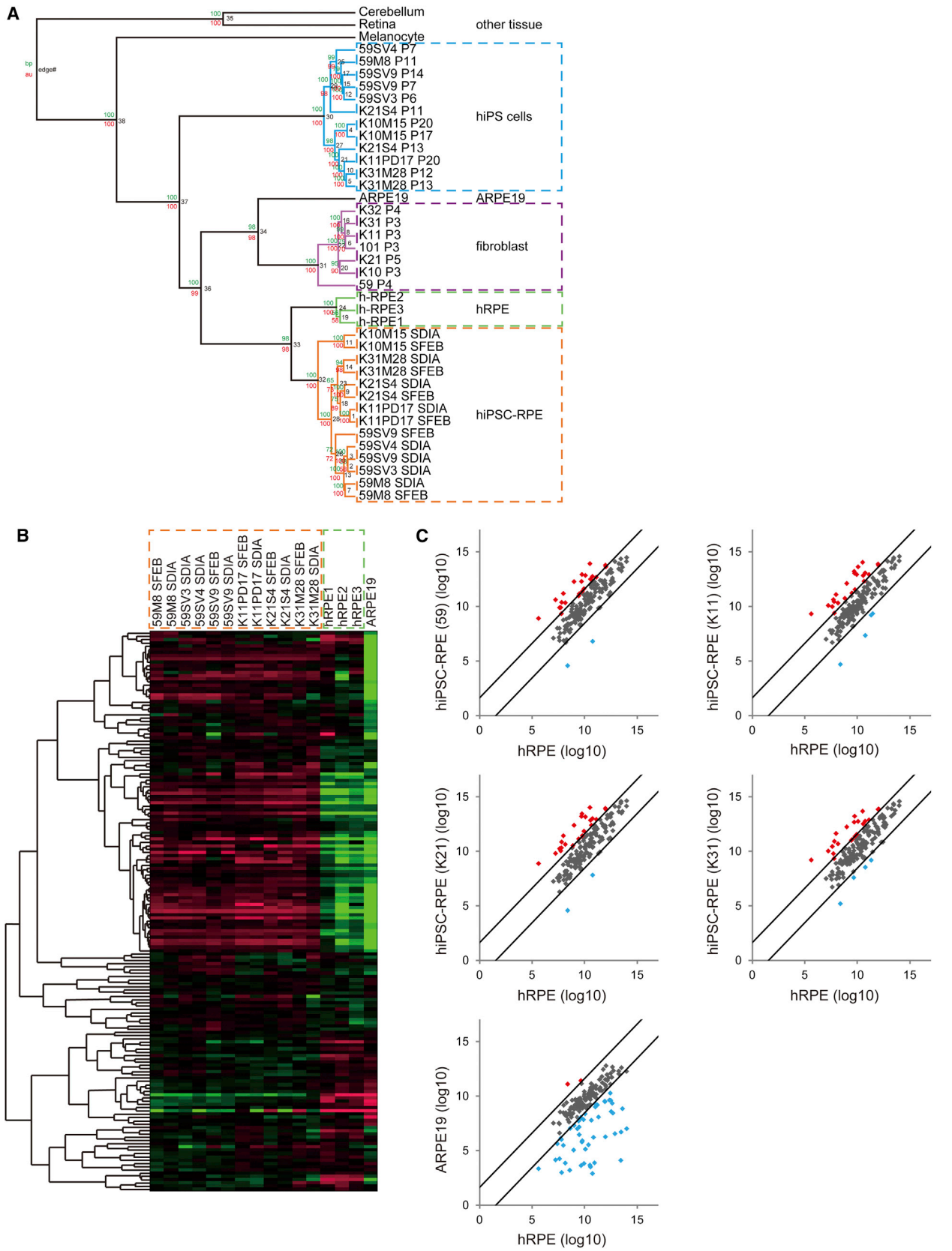

(legend on next page)

cells; dead cells: 0.10×10^4 cells; cell survival rate 93%, n = 24), or hiPSC-RPE cell suspension into the subretinal space of 3-week-old RCS rats. Six weeks later, we recorded electroretinograms (ERGs), and 9 weeks later, we measured the thickness of the retinal photoreceptor layer, i.e., the outer nuclear layer (ONL) (Figure 2D). RCS rats were administered cyclosporine to prevent rejection, and consequently no signs of rejection were observed around the transplantation sites. In nontransplanted eyes, the ONL was nearly completely lost, and immunostaining for rhodopsin was restricted to a debris zone of outer segments shed by the photoreceptors (Figure 2E). In contralateral eyes subjected to sham surgery, the ONL was approximately 1–2 cell rows thick and the outer limiting membrane containing ZO-1 was not detected (Figure 2F). In transplanted eyes, the ONL situated above hiPSC-RPE cell sheets, which is positive for EMMPRIN of human origin, was preserved with a thickness of five cell rows, and the ONL with the debris zone was preserved beyond the border of the graft (Figure 2G). The outer limiting membrane was also preserved around the graft. This result was consistent among the hiPSC-RPE cell sheets derived from any of the hiPSC lines tested. We also obtained similar results with transplantation of hiPSC-RPE cell suspension (253G1, 1.0×10^5 cells). ONL thickness in the transplanted RCS rat group was significantly greater than that in either the sham or the nontransplanted group (Figure 2H). In addition, transplantation of hiPSC-RPE cell sheet and cell suspension both significantly restored ERG responses in RCS rats (Figure 2I), and none of the transplanted cells showed tumor formation. These results indicate that hiPSC-RPE cell sheets show characteristics similar to those of native RPE both in vitro and in vivo.

Gene Expression of hiPSC-RPE

We previously generated hiPSCs from patients with RP using retrovirus (59M8, K10M15, K11PD17, K21S4, and K31M28) and Sendai virus (59SV3, 59SV4, and 59SV9) vectors, which we differentiated into hiPSC-RPE using two different methods (stromal cell-derived inducing activity [SDIA] [Kawasaki et al., 2002] and serum-free culture of embryoid body-like aggregates [SFEB] [Osakada et al., 2008; Watanabe et al., 2005]). To investigate whether these hiPSC-RPE colonies showed gene-expression patterns similar to those of native RPE, we classified hiPSC-RPE, hiPSCs, and fibroblasts from RP patients, hRPE, ARPE19 (a human RPE cell line), and other human tissues from 54,675 probe sets using microarray data. By performing hierarchical clustering analysis on these cells, we were able to generate a phylogenetic tree in which each cell type was separated independently and all hiPSC-RPEs were grouped near the native hRPE cluster (Figure 3A). All data are available from the Gene Expression Omnibus (GEO) repository at the National Center for Biotechnology Information (NCBI) archives Series (GSE50738, http://www.ncbi.nlm.nih.gov/geo/query/acc.cgi?acc=GSE50738).

We next examined the expression of 154 genes selected as RPE signature genes (Strunnikova et al., 2010) in 12 hiPSC-RPE lines, three hRPE lines, and ARPE19. Figure 3B shows a heatmap of the expression of these 154 genes in the above cell lines. All hiPSC-RPEs consistently showed similar patterns of gene expression irrespective of the patient or the methods used to generate the hiPSCs and induce their differentiation into RPE. We then compared the expression of these 154 genes in hiPSC-RPE or ARPE19 with hRPE as native RPE. The RPE signature genes in each hiPSC-RPE showed expression patterns serum-free suspension to that of hRPE, whereas many genes in ARPE19, including critical genes such as *RPE65* and *BEST1*, showed lower expression than those in hRPE lines (Figure 3C; Table S1).

Immunogenicity of iPSC-RPE In Vitro and In Vivo

A major cause of RPE transplantation failure in clinical practice is graft rejection; however, autologous grafts of hiPSC-RPE are expected to be nonimmunogenic, given

Figure 3. Gene Expression of hiPSC-RPE

(A) Phylogenetic tree of classified hiPSC-RPE, hiPSCs, and fibroblasts from RP patients, hRPE, ARPE19, and other human tissues from 54,675 probe sets using microarray data. The phylogenetic tree shows each cell type separated independently, with all hiPSC-RPE grouped near the native hRPE cluster. Bootstrap values are noted near the branches (maximum parsimony above and maximum likelihood below).

(B) Heatmap of 154 genes selected as RPE signature genes in 12 hiPSC-RPE lines, three hRPE lines, and ARPE19. All hiPSC-RPE lines consistently showed similar patterns of gene expression irrespective of the patient or the methods used to generate the hiPSCs and induce their differentiation into RPE.

(C) Scatterplot of normalized expression logarithmic values of the 154 genes in hiPSC-RPE (59, K11, K21, and K31) and ARPE19 compared with hRPE. Each gene is represented by a point (black point for the genes that do not change more than three times between the two cell populations; red and blue points for the genes that change more than three times between the two cell populations). hiPSC-RPE showed that almost all of the genes had similar expression (black points) with hRPE, and only two to four genes (blue points) had low expression levels. ARPE19 showed 116 genes with similar expression (black points), and 43 genes (blue points), including critical genes such as *RPE65* and *BEST1*, with lower expression.

See also Table S1.

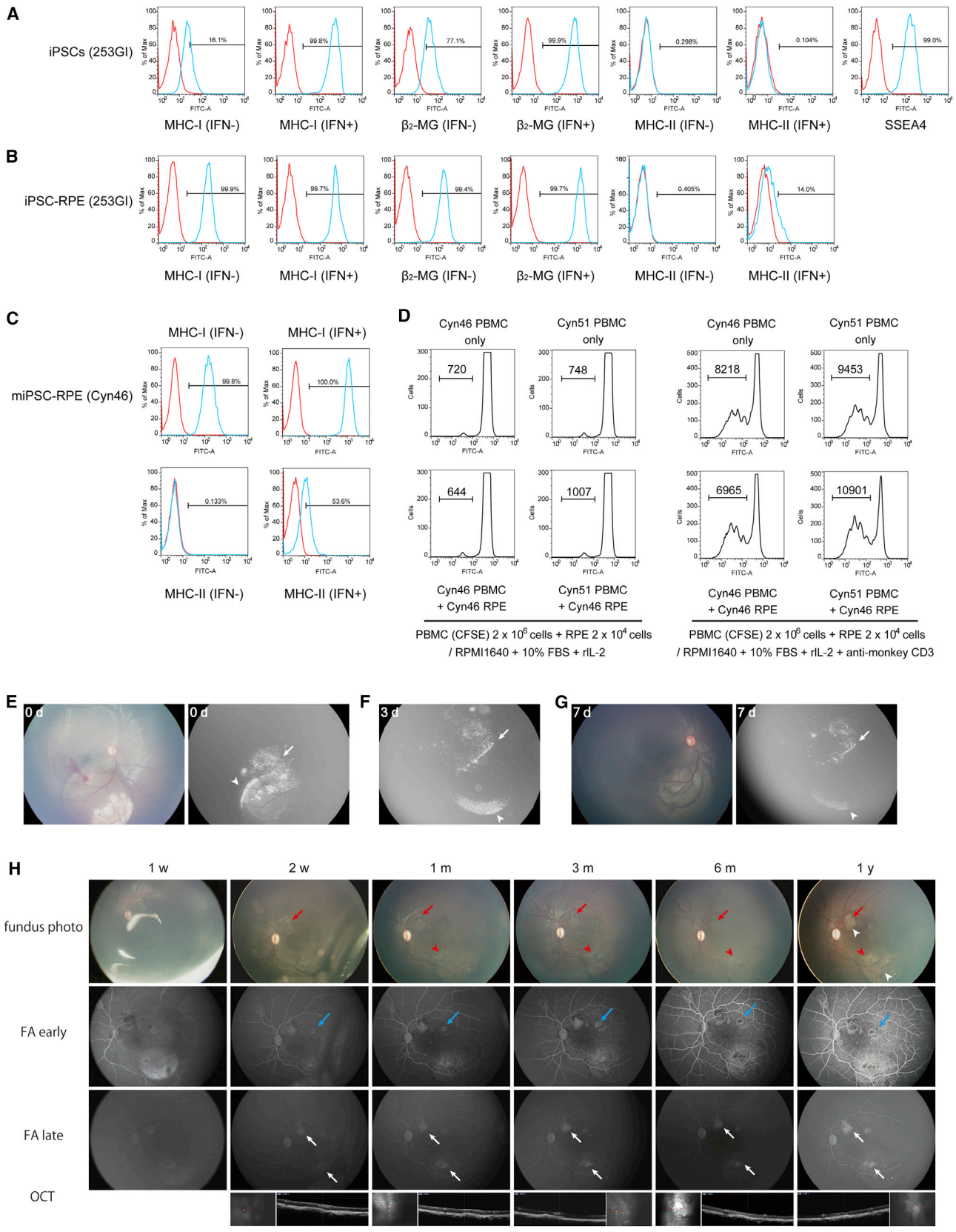

(legend on next page)

their presumably nearly identical genetic match to the recipient. We first examined the expression of major histocompatibility complex (MHC) proteins, which play an important role in mediating immune response, on the surfaces of graft cells to examine the potential immunogenicity of iPSC-RPE in vitro. hiPSCs expressed low levels of MHC class I (MHC-I) and β_2-microglobulin (β_2-MG) proteins (Figure 4A), which increased upon differentiation (Figure 4B). Since RPE transplantation surgery may induce some degree of inflammation, we examined the effect of the proinflammatory cytokine interferon-gamma (IFN-γ) on the surface expression of these proteins in hiPSCs and hiPSC-RPE. Addition of IFN-γ increased the expression of MHC-I and β_2-MG on hiPSCs (Figure 4A), and slightly upregulated the expression of MHC-II on hiPSC-RPE (Figure 4B). Other hiPSCs, hiPSC-RPE (59SV9), and hRPE yielded similar results (Figure S1). Hence, grafts of allogeneic hiPSC-RPE may be rejected in a manner similar to that observed in fetal RPE transplantation. We next prepared iPSC-RPE (Okamoto and Takahashi, 2011) from cynomolgus monkey (*Macaca fascicularis*) somatic cells (miPSC-RPE) and transplanted them into the eyes of recipient monkeys to examine the immunogenicity of iPSC-RPE in vitro and in vivo. We first examined the expression of MHC-I and MHC-II on miPSC-RPE (Cyn46). As expected, miPSC-RPE constitutively expressed MHC-I, but not MHC-II (Figure 4C). On the other hand, IFN-γ-treated miPSC-RPE expressed MHC-II. As next step, to confirm that the MHC mismatch between peripheral blood mononuclear cells (PBMCs) and allogeneic iPS-RPE cells in monkey were sufficient to elicit strong allogeneic responses, PBMCs were isolated from two monkeys (Cyn46 [autogenic] and Cyn51 [allogeneic]) and cultured with miPSC-RPE (Cyn46) in the presence or absence of anti-monkey CD3 antibody. To avoid nonspecific T cell proliferation, anti-CD3 antibodies were used after 24 hr of culture. The results showed that Cyn46 PBMCs did not induce proliferation of miPSC-RPE, whereas Cyn51 allogeneic PBMCs induced proliferation (Figure 4D), indicating that an MHC disparity between lymphocytes and allogeneic iPSC-RPE can induce immune responses. These results suggest that lymphocytes may directly attack MHC antigens on iPSC-RPE after transplantation. However, an MHC match between lymphocytes and RPE cannot induce immune responses. To date, RPEs have been clinically transplanted as either a cell suspension or RPE-choroid sheets. We compared the outcomes of miPSC-RPE cell suspension and cell sheets transplanted into the subretinal space in monkeys. For cell-suspension transplantation, we introduced Venus (a variant of yellow fluorescent protein) into miPSC-RPE using a lentivirus produced in 293T packaging cells (Miyoshi et al., 1998) to trace the transplanted miPSC-RPE after surgery using a fluorescein angiography (FA) camera. Although miPSC-RPE were observed in the macular area due to the supine position of the animals immediately following surgery (Figure 4E), these cells accumulated at the lower margin of the induced retinal detachment by 7 days after surgery (Figures 4F and 4G). In addition, some transplanted cells were refluxed into the vitreous cavity, which is major cause of proliferative vitreoretinopathy, a severe complication. In contrast, transplanted miPSC-RPE cell sheets were observed without Venus introduction after surgery, situated on the transplanted site. In RPE transplantation, cell sheets thus demonstrate a number of advantages, including graft control, less dispersion, and traceability.

We next transplanted 1 × 2 mm miPSC-RPE cell sheets as three allografts and one autograft into the subretinal space of four monkeys without immunosuppression and observed the monkeys for 1 year. Briefly, iPSCs were derived

Figure 4. Immunogenicity of iPSC-RPE In Vitro and In Vivo

(A–C) Mean fluorescence intensity of MHC antigens in hiPSCs (A; 253G1), hiPSC-RPE (B), and miPSC-RPE (C; Cyn46) with and without IFN-γ and pluripotency marker (SSEA4) in hiPSCs (A). The red line histograms represent isotype control antibodies. Numbers in the histogram indicate that the percentage of positive cells determined by isotype-specific control was less than 0.5%.

(D) Lymphocyte reactions of autogenic or allogeneic miPSC-RPE. miPSC-RPE (Cyn46) were cocultured with CFSE-labeled PBMCs from a Cyn46 autogenic or Cyn51 allogeneic monkey. In right panels, anti-monkey CD3 antibody was used in cultures for PBMCs plus iPS-RPE after 24 hr. CFSE-labeled PBMCs were analyzed by flow cytometry. Numbers in the histogram indicate CFSE-positive cells.

(E–G) Transplantation of miPSC-RPE cell suspension into the subretinal space of a monkey immediately following surgery (0d; E) and then 3 days (3d; F) and 7 days (7d; G) after surgery.

(E) Transplanted cells were observed in the macular area (arrowhead, right panel) using FA, and some transplanted cells were refluxed into the vitreous cavity (arrow, right panel). Transplanted cells could not be observed by color fundus photography after surgery (left panel).

(F and G) Transplanted cells accumulated at the lower margin of the induced retinal detachment by 7 days after surgery (arrowhead). Some transplanted cells refluxed into the vitreous cavity (arrow).

(H) Image of autologous miPSC-RPE cell sheet (red arrow) transplantation, showing depigmentation (around the red arrow) and moderate hyperfluorescence (white arrowhead) on FA around the engrafted graft, comparable to the hyperfluorescence commonly observed over artificial retinal detachment (red arrowhead) 1 year after surgery. The injection site (blue arrow) also showed moderate hyperfluorescence on FA.

See also Figures S1 and S2.

from a single animal and used to generate miPSC-RPE cell sheets; the iPSC donor also served as the sole autograft recipient (Cyn46). The other three monkeys (Cyn51, Cyn54, and P170), which were MHC mismatched to the iPSC donor, were transplanted with the allogeneic miPSC-RPE cell sheets. In the allograft, typical signs of graft rejection, such as formation of whitish fibrous tissues, leakage of fluorescein on FA, and hyperreflective material under the retina or retinal edema on optical coherence tomography (OCT), were detected around the grafts (Figure S2). In contrast, in the autograft transplant, we found only slight depigmentation of the engrafted RPE and moderate hyperfluorescence on FA around the graft, comparable to the hyperfluorescence commonly observed over artificial retinal detachment 1 year after surgery (Figure 4H). We conclude that the autograft showed no rejection signs and none of the transplanted cells showed tumor formation.

DISCUSSION

In this study, we report the production of hiPSC-RPE cell sheets without any artificial scaffold. These hiPSC-RPE cell sheets exhibit the morphological properties, in vitro and in vivo function, gene expression, and immunogenicity of authentic RPE, as well as the structural rigidity needed to withstand the physical stresses associated with the transplant procedure, suggesting they may show safety and utility suitable for human clinical research and application.

Considerable attention has been paid to the potential of hiPSCs as a cell source for regenerative medicine, disease modeling, and drug testing, and research into the use of PSC-derived cells in regenerative medicine has made rapid advances in recent years. Transplantation of RPE derived from PSCs for use in the potential treatment of diseases such as AMD represents a first-line research target in this field. The rationales underlying this approach include the following: (1) Limitations of the available treatments for AMD, such as anti-VEGF therapy and photodynamic therapy, which treat choroidal neovascularization but not the underlying RPE degeneration in advanced AMD, have led to attention being given to alternative approaches in which pathological RPE is replaced by healthy RPE. (2) RPE consist of pigmented cells that have a typical cobblestone appearance and form colonies during differentiation, thus providing visual cues to facilitate purification. (3) The number of cells needed for a lesion site is small compared with that needed for many other forms of proposed cell therapy (Mason and Dunnill, 2009). (4) iPS-RPE cells are readily functional in vitro and do not require specified integration into the neural network or further maturation in vivo. (5) Clinical studies of fetal or autologous RPE cell-sheet transplantation have shown some degree of efficacy, although problems of rejection (Algvere et al., 1994) or invasive harvesting (Binder et al., 2002; van Meurs and Van Den Biesen, 2003) remain. Transplantation of an RPE suspension derived from human ESCs, which are similar in many ways to hiPSCs, is being tested in a clinical trial (Strunnikova et al., 2010). Given these merits, we suggest that the generation of autologous RPE cell sheets that are very highly similar to native RPE in vitro may represent a very attractive option for cell transplantation therapy in AMD.

The hiPSC-RPE cell sheets made by our protocol are cellular monolayers and maintain their structure using both tight junctions and a basement-membrane-like structure that is positive for laminin and type IV collagen, which in native RPE collectively form the basement membrane. The collagen gel initially used to make hiPSC-RPE cell sheets is type I collagen, and the collagen gel was removed by the collagenase I treatment, which dissolves collagens I, II, and III, but not collagen IV, indicating that our grafts contain purely autonomously produced collagen IV and laminin. Several groups have reported the use of artificial scaffolds to maintain RPE cell sheets in monolayer, but biodegradable materials often cause inflammation, and nondegradable membranes may interfere with physiological interactions between the choroid and the RPE with overlying photoreceptors. Comparing RPE cell suspension with RPE cell sheet, a previous report showed that harvested autologous RPE suspension did not survive at the lesion site of AMD patients, while RPE around the harvested area proliferated and covered the defective area. The RPE and Bruch's membrane, including a collagen-, elastin-, and laminin-rich extracellular matrix in the lesion site of AMD patients, is impaired, suggesting that transplanted RPE need extracellular matrix, collagen IV, and laminin to engraft. In addition, grafts in the form of sheets have advantages in protecting cells from apoptosis and allowing the manipulative control of grafts, as shown in Figure 4. Thus, the hiPSC-RPE cell sheets with their own basement-membrane-like structure described in this report may offer advantages over RPE suspensions and RPE cell sheets with an artificial scaffold.

Our hiPSC-RPE cell sheets met general requirements, in terms of quality, quantity, consistency, and safety, for clinical-grade donor cells intended for use in cell replacement therapy. These cell sheets expressed typical RPE markers, showed polarized secretion of PEDF and VEGF, and exhibited phagocytotic activity similar to that of native RPE in vivo. With regard to graft survival, we confirmed that the grafted hiPSC-RPE cell sheets were positive for anti-human antibody for at least up to 9 weeks after

transplantation in immune-suppressed RCS rats. In terms of quantity, it is simple to obtain a sufficient amount of RPE from hiPSCs for transplantation into an AMD patient. Our protocol may require only a relatively small-scale culture system, which may also be an advantage considering the processes required in Good Manufacturing Practice (GMP) facilities. A hiPSC-RPE sheet with a diameter of 1 cm can be generated from 5×10^5 cells, which is sufficient to cover a macular area with a diameter of 3 mm. RPE generated by our protocol proved to be consistent, as shown by a cluster analysis of microarray data, in which hiPSC-RPE differentiated from various cell lines by various methods uniformly clustered in a group near that of human fetal RPE. Moreover, strikingly similar expression patterns of 154 RPE "hallmark" genes were observed in all 12 hiPSC-RPEs tested. In addition, 20 hallmark genes showed consistently higher expression levels in all 12 hiPSC-RPEs than in fetal RPE. Nine of these genes, including two mature RPE genes (*RPE65* and *BEST1*), indicated the developmental stage, which was reported to be more highly expressed in adult native RPE than in fetal native RPE (Strunnikova et al., 2010). Conversely, two genes that had higher expression in fetal native RPE (*COL8A2*, which affects collagen type VIII, and *DCT*, which affects biosynthesis of melanin) did not seem to have a relation to RPE maturation. These results indicate that hiPSC-RPE is nearer to the adult RPE stage. Lastly, safety remains the major concern confronting the development of hiPSC-derived clinical products, as contamination of grafts by residual hiPSCs may result in the formation of teratomas, a form of benign tumor. We were able to purify RPE efficiently by a series of "pick up and expand" procedures, taking advantage of RPE cells' unique morphology. Furthermore, to our knowledge, there have been no reports in the literature of tumors of RPE origin. To confirm that hiPSC-RPE purified by our method showed no contamination by significant numbers of hiPSCs, we used quantitative PCR of Lin28. This method is capable of detecting a single iPSC from a 50,000-cell colony (Kuroda et al., 2012), which is significantly lower than the number of undifferentiated cells needed to induce tumor formation (data not shown). We also did not observe any tumor formation in vivo following injection of purified hiPSC-RPE cell sheets and suspension in RCS rats for 9 weeks, hiPSC-RPE cell sheets in monkeys for 1 year (Figures 2 and 4), or 1 × 1 mm hiPSC-RPE cell sheets in the subretinal space of immunodeficient mice for 60 weeks (H.Kanemura, M. Go, M. Shikamura, N. Nishihita, N. Sakai, H.K., M. Mandai, M. Takahashi, and S. Kawamata, unpublished data).

Once the use of hiPSC-derived RPE has been justified in clinical practice, a variety of customized transplantation approaches may be developed in the future. For diseases such as exudative AMD, in which the blood-retinal barrier is disrupted, autografts derived from the recipient would presumably be more suitable. There may also be cases, such as RPE tear, in which allograft transplantation would be more appropriate. The use of selected cell lines would also clearly be more cost-efficient in the event that demand for cell transplants increases. The ocular space has historically been thought of as an immunoprivileged site, and in pathologies in which barrier function is maintained, allografts may be accepted by the host tissue, as evidenced by reports that human fetal RPE (Algvere et al., 1994) and hESC-RPE (Schwartz et al., 2012) transplants in patients with dry-type AMD and Stargardt's disease were not rejected. For these purposes, a cell bank of iPSC lines with multiple human leukocyte antigen types may provide a good system for more widespread applications of RPE transplantation. In addition, advances in clinical imaging techniques, such as OCT and fundus autofluorescence (Schmitz-Valckenberg et al., 2009), have enabled the detection of early pathologic changes. In cases in which hESCs or hiPSC-RPE cells are transplanted for early dry-type AMD or for prevention of wet-type AMD, for instance, transplantation of RPE cell suspension may be a better option, in order to minimize surgical invasion. Cell suspension had an equivalent effect in our data (Figure 2H), and the effect may reflect the coverage area of transplanted cells (Figure 2I). Additionally, RPE cell sheets using artificial scaffolds may one day be engineered to provide additional benefits, such as the secretion of supplemental neurotrophic factors.

In summary, the advantages of our RPE cell sheets in comparison with cell suspension include morphological and physiological similarities to native RPE, solid coverage of the lesion, and traceability after transplantation; however, we still need to scale up and reduce the costs of manufacturing. Additionally, the avoidance of artificial scaffolds is ideal, since artificial scaffolds often cause inflammation. The use of auto-hiPSCs provides the advantage of minimizing the risk of graft rejection, especially in diseases with a disrupted blood-retinal barrier, such as wet-type AMD. A disadvantage of sheet transplantation compared with cell-suspension transplantation is that it requires a more complicated, invasive surgical procedure, and we are trying to resolve this issue by refining the transplantation method.

We recently finished preparing hiPSC-RPE cell sheets in a GMP-grade cell-processing facility based on the method described in this study, and confirmed the consistent reproducibility of the results, as well as the safety of the cell sheets for clinical application. We hope that the preliminary data shown in the present study provide useful information for the advancement of future RPE replacement therapies.

EXPERIMENTAL PROCEDURES

Culture of hiPSCs and hiPSC-RPE

The methods used for hiPSC maintenance and differentiation were described previously (Haruta et al., 2004; Kawasaki et al., 2002; Osakada et al., 2008). The hiPSC line 253G1 (Nakagawa et al., 2008), made from healthy human dermal fibroblast cells, was purchased from RIKEN BioResource Center. Another iPSC line was made by our group from dermal fibroblasts of a patient with RP (with a photoreceptor-specific gene mutation) by retroviral (59M8, K10, K11, K21, and K31) and Sendai viral (59SV3, 59SV4, and 59SV9) introduction of OCT3/4, SOX2, c-MYC, and KLF4, and maintained as previously described (Jin et al., 2012). For details, see Supplemental Experimental Procedures.

Culture of Nonhuman Primate iPSCs and iPSC-RPE

miPSCs and iPSC-RPE were made from cynomolgus monkeys (Japan Biological Science) as previously described using OCT3/4, SOX2, c-MYC, and KLF (Okamoto and Takahashi, 2011). For details, see Supplemental Experimental Procedures.

Preparation of Human and Nonhuman Primate iPSC-RPE Cell Sheets without any Artificial Scaffold

Collagen gel was prepared on ice using the Collagen Gel Culture Kit (Nitta Gelatin) according to the manufacturer's instructions. Briefly, acid-solubilized porcine tendon collagen type I-A (3 mg/ml, Cellmatrix; Nitta Gelatin), 5× concentrated Dulbecco's modified Eagle's medium (DMEM; Nitta Gelatin), and reconstitution buffer (NaOH 50 mM, $NaHCO_3$ 260 mM, HEPES 200 mM; Nitta Gelatin) were gently mixed in a ratio of 7:2:1 on ice, and this collagen solution was added on the Transwell insert, polymerized at 37°C for 30 min, and incubated in RPE cell sheet medium (F10 culture medium [Sigma] and 10% fetal bovine serum) overnight. The next day, iPSC-RPE (5×10^5 cells/500 μl/well) were seeded on the collagen gel and cultured in RPE cell sheet medium. After reaching confluence, the iPSC-RPE were cultured in serum-free retinal medium supplemented with 10 ng/ml basic fibroblast growth factor and SB431542 (0.5 μM) for at least 4 weeks. The medium was changed every 2–3 days.

To prepare iPSC-RPE cell sheets without any artificial scaffold, we removed the insert membrane and applied a collagenase I (Roche) at 37°C for 30 min to dissolve the collagen gel, and then cut the margin of the hiPSC-RPE to release it from the insert as an intact cell sheet. The hiPSC-RPE cell sheets were washed in PBS and transferred to a dish for LMD (Lumox-35; Greiner). These sheets were kept moist with DMEM/F12 (200 μl) until they were cut using LMD (PALM MicroBeam; Zeiss) according to the manufacturer's instructions.

Microarrays

RNA was extracted from hiPSC-RPE, hRPE, ARPE19, hiPSCs, and fibroblasts using TRIzol (Invitrogen) and purified by RNeasy (QIAGEN). Labeled aRNA was generated from total RNA using a 3′ IVT Express Kit (Affymetrix) and then hybridized to expression microarrays (Human Genome U133 Plus 2.0 Array; Affymetrix). Labeling, hybridization, signal detection, and analysis were performed by the CDB Gene Chip Service. hRPE (hRPE1, lot-0F3237; hRPE2, lot-0F32920; and hRPE3, lot-181239) were purchased from Lonza. For further details, see the GEO database (Series GSE50738, http://www.ncbi.nlm.nih.gov/geo/query/acc.cgi?acc=GSE50738).

Animal Experiments

The care and maintenance of the rats conformed to the ARVO statements for the Use of Animals in Ophthalmic and Vision Research, and the Use of Laboratory Animals, as well as the Guidelines of the RIKEN CDB Animal Experiment Committee. The animals were housed in rooms under standard laboratory conditions (18–23°C, 40%–65% humidity, 12 hr light/12 hr dark cycle), with food and water available ad libitum. Animals were anesthetized with a mixture of ketamine and xylazine, and their pupils were dilated with 0.5% tropicamide and 0.5% phenylephrine hydrochloride.

Transplantation of hiPSC-RPE Cell Sheets into the Subretinal Space of RCS Rats

Pink-eyed dystrophic RCS (Jcl-rdy/rdy, p-) rats were purchased from CLEA Japan and maintained as described previously (Haruta et al., 2004). For transplantation, we made a small scleral incision using a 30-gauge disposable needle. Then, we injected 2 μl DMEM/F12 (50:50) medium including a fragment of 1 × 1 mm hiPSC-RPE cell sheets, hiPSC-RPE cell suspension including 1×10^5 cells, or medium only as sham injection into the subretinal space of the right eye of RCS rats using a 33-gauge needle. An equivalent volume of DMEM/F12 medium was injected subretinally as sham surgery in eight contralateral eyes. The other contralateral eyes were classified as "no treatment." Nine weeks after transplantation (i.e., at 12 weeks age), the eyes were processed for histological evaluation. RCS rats were administered cyclosporine to prevent rejection, and consequently no signs of rejection were observed around the transplantation sites.

Transplantation of miPSC-RPE Cell Suspension and Cell Sheets into the Subretinal Space in Monkeys

Cynomolgus monkeys were purchased from Japan Biological Science. miPSC-RPE were labeled with Venus produced from a self-inactivating HIV-1-based lentivirus vector, CS-CDF-CMV-Venus-PRE.

For transplantation of miPSC-RPE cell suspension, 5×10^4 cells in 100 μl DMEM/F12 medium were injected into the subretinal space. These cells were monitored through the FA barrier filter of a color fundus camera (RetCamII; Clarity) immediately and then 3 and 7 days after surgery.

For transplantation of miPSC-RPE cell sheets, after induction of a posterior vitreous detachment by active suction, a complete vitrectomy (Accurus; Alcon) was performed. A localized retinal detachment was created by intraocular irrigating solution (BSS Plus; Alcon) using a subretinal injection cannula (rigid injection cannula; Synergetics). The transplantation site was enlarged to enable implantation of graft, and another retinotomy site for drainage was created by diathermy. A 1 × 2 mm graft in DMEM/F12 medium was transplanted using an outer tube of a 20-gauge indwelling needle (Terumo) attached to an extension tube (fluid tubing extension kit; Eagle) of a 1 ml syringe (Terumo). After draining subretinal

fluid with brush aspiration (DORC) with the help of perfluorocarbon liquid (Alcon), we performed fluid-air exchange and perfluoropane (ISPAN C_3F_8; Alcon) tamponade. These grafts were monitored by means of color fundus pictures and FA (RetCamII; Clarity) and OCT (Nidek) at 1, 2, and 4 weeks; 3 and 6 months; and 1 year after surgery.

Statistical Analysis

The values are expressed as mean ± SEM, with $p < 0.05$ being considered statistically significant. Secretion of PEDF and VEGF was evaluated using paired t tests. One-way ANOVA followed by Scheffe's test was performed to compare the maximum ONL thickness and b-wave amplitudes of ERG among nontransplanted, sham-transplanted, and transplanted animals to evaluate the efficacy of treatment. Probability values < 5% were considered significant.

For further details regarding the experimental procedures used in this work, including cell culture, immunocytochemistry, immunohistochemistry, transmission electron microscopy, RT-PCR, ELISA, fluorescence-activated cell sorting (FACS), TER, and ERG, see Supplemental Experimental Procedures.

SUPPLEMENTAL INFORMATION

Supplemental information includes Supplemental Experimental Procedures, two figures, one table, and three movies, and can be found with this article online at http://dx.doi.org/10.1016/j.stemcr.2013.12.007.

AUTHOR CONTRIBUTIONS

H.K. generated RPE cell sheets without any artificial cell sheets and performed subretinal injection into RCS rats. M.M. conducted subretinal transplantation into monkeys. S.O. performed culture of nonhuman primate iPSCs and iPSC-RPE. N.S. performed culture of hiPSCs and hiPSC-RPE. A.S. analyzed gene-expression data with T. Kasukawa. S.S. conducted FACS of nonhuman primate iPSCs and iPSC-RPE. J.K. supervised subretinal transplantation. M.T. supervised all experiments.

ACKNOWLEDGMENTS

We thank Y. Kurimoto and Y. Hirami for providing skin samples from patients with RP; T. Kasukawa for analyzing the gene expression of hiPSC-RPE; T. Yasukawa for valuable comments on this work; C. Yamada, K. Iseki, Y. Wataoka, and K. Sadamoto for excellent technical assistance; and members of the Takahashi laboratory for discussions. This study was supported by a grant from the Project for Realization of Regenerative Medicine, MEXT.

Received: September 6, 2013
Revised: December 11, 2013
Accepted: December 11, 2013
Published: January 23, 2014

REFERENCES

Adamis, A.P., Shima, D.T., Yeo, K.T., Yeo, T.K., Brown, L.F., Berse, B., D'Amore, P.A., and Folkman, J. (1993). Synthesis and secretion of vascular permeability factor/vascular endothelial growth factor by human retinal pigment epithelial cells. Biochem. Biophys. Res. Commun. *193*, 631–638.

Algvere, P.V., Berglin, L., Gouras, P., and Sheng, Y. (1994). Transplantation of fetal retinal pigment epithelium in age-related macular degeneration with subfoveal neovascularization. Graefes Arch. Clin. Exp. Ophthalmol. *232*, 707–716.

Bhatt, N.S., Newsome, D.A., Fenech, T., Hessburg, T.P., Diamond, J.G., Miceli, M.V., Kratz, K.E., and Oliver, P.D. (1994). Experimental transplantation of human retinal pigment epithelial cells on collagen substrates. Am. J. Ophthalmol. *117*, 214–221.

Binder, S., Stolba, U., Krebs, I., Kellner, L., Jahn, C., Feichtinger, H., Povelka, M., Frohner, U., Kruger, A., Hilgers, R.D., and Krugluger, W. (2002). Transplantation of autologous retinal pigment epithelium in eyes with foveal neovascularization resulting from age-related macular degeneration: a pilot study. Am. J. Ophthalmol. *133*, 215–225.

Bressler, N.M., Bressler, S.B., and Fine, S.L. (1988). Age-related macular degeneration. Surv. Ophthalmol. *32*, 375–413.

Dowling, J.E., and Sidman, R.L. (1962). Inherited retinal dystrophy in the rat. J. Cell Biol. *14*, 73–109.

Gal, A., Li, Y., Thompson, D.A., Weir, J., Orth, U., Jacobson, S.G., Apfelstedt-Sylla, E., and Vollrath, D. (2000). Mutations in MERTK, the human orthologue of the RCS rat retinal dystrophy gene, cause retinitis pigmentosa. Nat. Genet. *26*, 270–271.

Gu, S.M., Thompson, D.A., Srikumari, C.R., Lorenz, B., Finckh, U., Nicoletti, A., Murthy, K.R., Rathmann, M., Kumaramanickavel, G., Denton, M.J., and Gal, A. (1997). Mutations in RPE65 cause autosomal recessive childhood-onset severe retinal dystrophy. Nat. Genet. *17*, 194–197.

Harimoto, M., Yamato, M., Hirose, M., Takahashi, C., Isoi, Y., Kikuchi, A., and Okano, T. (2002). Novel approach for achieving double-layered cell sheets co-culture: overlaying endothelial cell sheets onto monolayer hepatocytes utilizing temperature-responsive culture dishes. J. Biomed. Mater. Res. *62*, 464–470.

Haruta, M., Sasai, Y., Kawasaki, H., Amemiya, K., Ooto, S., Kitada, M., Suemori, H., Nakatsuji, N., Ide, C., Honda, Y., and Takahashi, M. (2004). In vitro and in vivo characterization of pigment epithelial cells differentiated from primate embryonic stem cells. Invest. Ophthalmol. Vis. Sci. *45*, 1020–1025.

Hirami, Y., Osakada, F., Takahashi, K., Okita, K., Yamanaka, S., Ikeda, H., Yoshimura, N., and Takahashi, M. (2009). Generation of retinal cells from mouse and human induced pluripotent stem cells. Neurosci. Lett. *458*, 126–131.

Jin, Z.-B., Okamoto, S., Xiang, P., and Takahashi, M. (2012). Integration-free induced pluripotent stem cells derived from retinitis pigmentosa patient for disease modeling. Stem Cells Transl. Med. *1*, 503–509.

Kawasaki, H., Suemori, H., Mizuseki, K., Watanabe, K., Urano, F., Ichinose, H., Haruta, M., Takahashi, M., Yoshikawa, K., Nishikawa, S., et al. (2002). Generation of dopaminergic neurons and pigmented epithelia from primate ES cells by stromal cell-derived inducing activity. Proc. Natl. Acad. Sci. USA *99*, 1580–1585.

Kuroda, T., Yasuda, S., Kusakawa, S., Hirata, N., Kanda, Y., Suzuki, K., Takahashi, M., Nishikawa, S., Kawamata, S., and Sato, Y.

(2012). Highly sensitive in vitro methods for detection of residual undifferentiated cells in retinal pigment epithelial cells derived from human iPS cells. PLoS ONE *7*, e37342.

Lee, C.J., Huie, P., Leng, T., Peterman, M.C., Marmor, M.F., Blumenkranz, M.S., Bent, S.F., and Fishman, H.A. (2002). Microcontact printing on human tissue for retinal cell transplantation. Arch. Ophthalmol. *120*, 1714–1718.

Li, L.X., and Turner, J.E. (1988). Inherited retinal dystrophy in the RCS rat: prevention of photoreceptor degeneration by pigment epithelial cell transplantation. Exp. Eye Res. *47*, 911–917.

Marlhens, F., Bareil, C., Griffoin, J.-M., Zrenner, E., Amalric, P., Eliaou, C., Liu, S.-Y., Harris, E., Redmond, T.M., Arnaud, B., et al. (1997). Mutations in RPE65 cause Leber's congenital amaurosis. Nat. Genet. *17*, 139–141.

Mason, C., and Dunnill, P. (2009). Quantities of cells used for regenerative medicine and some implications for clinicians and bioprocessors. Regen. Med. *4*, 153–157.

Maw, M.A., Kennedy, B., Knight, A., Bridges, R., Roth, K.E., Mani, E.J., Mukkadan, J.K., Nancarrow, D., Crabb, J.W., and Denton, M.J. (1997). Mutation of the gene encoding cellular retinaldehyde-binding protein in autosomal recessive retinitis pigmentosa. Nat. Genet. *17*, 198–200.

Miyoshi, H., Blömer, U., Takahashi, M., Gage, F.H., and Verma, I.M. (1998). Development of a self-inactivating lentivirus vector. J. Virol. *72*, 8150–8157.

Mullen, R.J., and LaVail, M.M. (1976). Inherited retinal dystrophy: primary defect in pigment epithelium determined with experimental rat chimeras. Science *192*, 799–801.

Nakagawa, M., Koyanagi, M., Tanabe, K., Takahashi, K., Ichisaka, T., Aoi, T., Okita, K., Mochiduki, Y., Takizawa, N., and Yamanaka, S. (2008). Generation of induced pluripotent stem cells without Myc from mouse and human fibroblasts. Nat. Biotechnol. *26*, 101–106.

Nishida, K., Yamato, M., Hayashida, Y., Watanabe, K., Yamamoto, K., Adachi, E., Nagai, S., Kikuchi, A., Maeda, N., Watanabe, H., et al. (2004). Corneal reconstruction with tissue-engineered cell sheets composed of autologous oral mucosal epithelium. N. Engl. J. Med. *351*, 1187–1196.

Okamoto, S., and Takahashi, M. (2011). Induction of retinal pigment epithelial cells from monkey iPS cells. Invest. Ophthalmol. Vis. Sci. *52*, 8785–8790.

Osakada, F., Ikeda, H., Mandai, M., Wataya, T., Watanabe, K., Yoshimura, N., Akaike, A., Sasai, Y., and Takahashi, M. (2008). Toward the generation of rod and cone photoreceptors from mouse, monkey and human embryonic stem cells. Nat. Biotechnol. *26*, 215–224.

Schmitz-Valckenberg, S., Fleckenstein, M., Scholl, H.P.N., and Holz, F.G. (2009). Fundus autofluorescence and progression of age-related macular degeneration. Surv. Ophthalmol. *54*, 96–117.

Schwartz, S.D., Hubschman, J.-P., Heilwell, G., Franco-Cardenas, V., Pan, C.K., Ostrick, R.M., Mickunas, E., Gay, R., Klimanskaya, I., and Lanza, R. (2012). Embryonic stem cell trials for macular degeneration: a preliminary report. Lancet *379*, 713–720.

Shimizu, T., Yamato, M., Kikuchi, A., and Okano, T. (2001). Two-dimensional manipulation of cardiac myocyte sheets utilizing temperature-responsive culture dishes augments the pulsatile amplitude. Tissue Eng. *7*, 141–151.

Steele, F.R., Chader, G.J., Johnson, L.V., and Tombran-Tink, J. (1993). Pigment epithelium-derived factor: neurotrophic activity and identification as a member of the serine protease inhibitor gene family. Proc. Natl. Acad. Sci. USA *90*, 1526–1530.

Stevenson, B.R., Siliciano, J.D., Mooseker, M.S., and Goodenough, D.A. (1986). Identification of ZO-1: a high molecular weight polypeptide associated with the tight junction (zonula occludens) in a variety of epithelia. J. Cell Biol. *103*, 755–766.

Stone, E.M., Nichols, B.E., Streb, L.M., Kimura, A.E., and Sheffield, V.C. (1992). Genetic linkage of vitelliform macular degeneration (Best's disease) to chromosome 11q13. Nat. Genet. *1*, 246–250.

Strunnikova, N.V., Maminishkis, A., Barb, J.J., Wang, F., Zhi, C., Sergeev, Y., Chen, W., Edwards, A.O., Stambolian, D., Abecasis, G., et al. (2010). Transcriptome analysis and molecular signature of human retinal pigment epithelium. Hum. Mol. Genet. *19*, 2468–2486.

Takahashi, K., Tanabe, K., Ohnuki, M., Narita, M., Ichisaka, T., Tomoda, K., and Yamanaka, S. (2007). Induction of pluripotent stem cells from adult human fibroblasts by defined factors. Cell *131*, 861–872.

Tezel, T.H., and Del Priore, L.V. (1997). Reattachment to a substrate prevents apoptosis of human retinal pigment epithelium. Graefes Arch. Clin. Exp. Ophthalmol. *235*, 41–47.

Thomson, J.A., Itskovitz-Eldor, J., Shapiro, S.S., Waknitz, M.A., Swiergiel, J.J., Marshall, V.S., and Jones, J.M. (1998). Embryonic stem cell lines derived from human blastocysts. Science *282*, 1145–1147.

van Meurs, J.C., and Van Den Biesen, P.R. (2003). Autologous retinal pigment epithelium and choroid translocation in patients with exudative age-related macular degeneration: short-term follow-up. Am. J. Ophthalmol. *136*, 688–695.

Watanabe, K., Kamiya, D., Nishiyama, A., Katayama, T., Nozaki, S., Kawasaki, H., Watanabe, Y., Mizuseki, K., and Sasai, Y. (2005). Directed differentiation of telencephalic precursors from embryonic stem cells. Nat. Neurosci. *8*, 288–296.

Young, R.W., and Bok, D. (1969). Participation of the retinal pigment epithelium in the rod outer segment renewal process. J. Cell Biol. *42*, 392–403.